IEEE Access
Multidisciplinary | Rapid Review | Open Access Journal

Received 12 April 2023, accepted 26 April 2023, date of publication 1 May 2023, date of current version 9 May 2023.

Digital Object Identifier 10.1109/ACCESS.2023.3272000

RESEARCH ARTICLE

Coordination of Enhanced Control Schemes for Optimal Operation and Ancillary Services of Grid-Tied VSWT System

HUSSEIN SHUTARI[1], TAIB IBRAHIM[1], NURSYARIZAL BIN MOHD NOR[1], HAKIM Q. A. ABDULRAB[1], (Graduate Student Member, IEEE), NORDIN SAAD[2], (Senior Member, IEEE), AND QASEM AL-TASHI[3]

[1]Department of Electrical and Electronic Engineering, Universiti Teknologi PETRONAS, Seri Iskandar 32610, Malaysia
[2]Faculty of Computing and Engineering, Quest International University, Ipoh, Perak 30250, Malaysia
[3]Department of Imaging Physics, The University of Texas MD Anderson Cancer Center, Houston, TX 77030, USA

Corresponding author: Hussein Shutari (hussein_20000028@utp.edu.my)

This work was supported in part by the Ministry of Higher Education Malaysia and Universiti Teknologi PETRONAS (UTP) for the award of Fundamental Research Grant Project (FRGS) under Grant FRGS/1/2019/TK04/UTP/02/10, and in part by the UTP Graduate Research Assistantship Scheme.

ABSTRACT Wind power's increasing use and its integration into the utility grid have prompted scholars to focus more on the refinement of wind power harvesting systems, injecting stable power and providing ancillary services to the utility grid. This article introduces a novel hybrid approach termed as sine cosine algorithm and transient search optimization (HSCATSO) optimizer of better exploration and exploitation phases for optimal designing the power electronic converter control schemes (PECCS) of the grid-tied variable speed wind turbine (VSWT) system. The PECCS is simultaneously coordinated with a robust maximum power extraction algorithm (MPEA) to form enhanced control systems for achieving the best wind harnessing, improving the VSWT system performance, and supporting the utility grid stability. In this context, the HSCATSO optimally designs the PECCS parameters based on minimizing the summation of integral squared error (ISE) of multiple error signals in the developed control schemes in coordination with the MPEA. The superiority of the HSCATSO optimizer is validated using twenty benchmark functions and statistically analysed against four well-known optimization algorithms. Meanwhile, the effectiveness of the optimally designed PECCS using the HSCATSO is verified by the extensive simulation analysis in MATLAB/Simulink considering severe grid disturbance and real wind speed data taken from Kudat, Sabah, Malaysia to mimic realistic circumstances. The obtained results have been compared with that realized using the other algorithms-based design PECCS. The simulation outcomes affirmed that the PECCS designed by the HSCATSO and coordinated with MPEA resulted in higher power harvesting and enhanced the grid-tied VSWT system stability better than the competitive control schemes.

INDEX TERMS Power electronic converter control, PMSG, MPPT, maximum power extraction, PI controller tuning, wind power, sine cosine algorithm, transient search optimization, WECS, VSWT system.

I. INTRODUCTION

The rapid global population growth, technological improvements, and industrialization have all led to a rise in energy consumption in recent years. This consumption results in a substantial rise in energy generation, primarily dependent on fossil fuel supply [1]. Increased reliance on fossil fuels adversely impacts climate change, global warming and international's trade imbalance. In light of these challenges, decision-makers and utilities are now compelled to investigate more renewable energy sources to produce cheap, sustainable, and environmentally friendly electricity. Wind energy production is among the most rapidly expanding renewable energy technologies [2]. This is because of its

The associate editor coordinating the review of this manuscript and approving it for publication was Meng Huang.

TABLE 1. List of Abbreviations.

WECS	Wind Energy Conversion System
WT	Wind Turbine
VSWT	Variable Speed Wind Turbine
PMSG	Permanent Magnet Synchronous Generator
FSPEC	Full Scale Power Electronic Converter
GSR	Generator Side Rectifier
GSI	Grid side Inverter
MPEA	Maximum Power Extraction Algorithm
UG	Utility Grid
TSR	Tip Speed Ratio
PI	Proportional-Integral
SCA	Sine Cosine Algorithm
TSO	Transient Search Optimization
HSCATSO	Hybrid SCA and TSO
GWO	Grey Wolf Optimizer
PSO	Particle Swarm Optimization
ISE	Integral Squared Error
ODPI	Optimal Designed Proportional-Integral
LVRT	Low Voltage Ride Through

commercial advantages, environmental friendliness, and frequently large power output [3]. By 2022, when new turbines were put in place, the world's total amount of wind power capacity was 840.9 GW. This represents an increase of 96.5 GW compared to the record set in 2021. Moreover, recent estimates say that wind energy installations will be more than 917 GW worldwide by 2030 [4].

The WECS has undergone significant advancements during the wind energy sector's rapid expansion [5]. The WT is deemed an essential element of the WECS, and it is classed into VSWT and fixed speeds WT [6]. The VSWT, which is based on the PMSG and utilizes an FSPEC topology has been embraced by the majority of the wind turbine manufacturing sectors. This is because of its multiple advantageous characteristics, including its ability to maximize wind power, high efficiency, reduced power fluctuation, gear-less design, self-excitation, and reduced mechanical stress [7], [8], [9]. Besides, this design decouples the PMSG from the utility grid via FSPEC. Thus, grid fluctuation and disruptions do not affect the PMSG-VSWT system. In the typical implementation, the FSPEC that connects the PMSG-VSWT system with UG consists of a GSR and GSI joined to each other via DC-link capacitors and are also controlled by related control schemes called the MPEA, GSR control scheme, and GSI control schemes [10], [11]. Due to the randomness and intermittent characteristics of wind energy, the control schemes of FSPEC must be efficiently developed in a single framework to ensure power production optimally, comply with the grid's voltage and frequency stability, and guarantee power quality as ancillary services to UG operators to retain a stable electricity system.

When it comes to the control schemes, a cascaded vector control system is commonly used to control both the GSR and the GSI [12]. This cascaded vector control scheme is either based on adaptive neural network controllers, slide mode control, fuzzy logic control, model predictive control or traditional PI Controllers [13]. However, due to their complex computations and behaviour constraints, the implementation of slide mode control, fuzzy logic control, model predictive control and adaptive neural network controllers in the wind power industry is limited [14], [15], [16]. Hence, The PIs are still commonly deployed in a range of industrial applications due to their many beneficial properties, including their ease of use, long lifespan, and significant stability ranges [17]. Nevertheless, the PI controllers, on the other hand, are extremely sensitive to the parameter variations, non-linearity characteristics, and uncertainty of the systems [18]. In the body of research that has been done so far, various approaches have been put forward for suitably determining the gains of PI controllers [19]. In most of those techniques, designing such a controller depends on criteria that involve a process of experimentation and refinement, which requires a great deal of effort, is time-consuming, and primarily depends on the designer's level of expertise [20]. Therefore, optimal-designing PI controllers present serious challenges to control designers, especially in WECS, where it is difficult to present mathematical models or transfer functions. Consequently, numerous meta-heuristic algorithms have been used recently to optimal-design the cascaded PI controllers' gain for improving the grid-connected PMSG-VSWT system performance [21]. Some examples of the algorithms used include the adaptive filtering algorithm [22], symbiotic optimization algorithm [23], bacterial foraging optimization [24], optimal transient search algorithm [25], whale optimization algorithm [26], grey wolf optimizer [27], democratic joint operations algorithm [28], water cycle algorithm [29], particle swarm optimization algorithm [30], augmented grey wolf optimizer [31], gravitational search algorithm [32] and Sine Cosine Algorithm [33].

Moreover, in [34] the Elephant herding algorithm is introduced to fine-tune the gain of the PI controller for controlling the off-delay angle of a synchronous reluctance generator in WECS to improve its ability to meet LVRT requirements under varying wind speeds and system faults. Significant performance improvements can be achieved for grid-tied VSWT systems when optimization approaches such as those stated above are utilised.

In the domain of optimizing the VSWT control system, a previous study [33] demonstrated that the SCA algorithm outperformed other competitive algorithms in finding optimal solutions and was suitable for addressing optimization problems. However, SCA tends to become trapped in local optima and fail to converge in certain complex cases, which aligns with the No-Free-Lunch theorem that asserts no single algorithm can exhibit superior performance over others in solving all optimization problems. Therefore, there remains a need to enhance the performance and efficiency of the original SCA algorithm in some manner and apply it to a specific purpose.

In this work, a novel efficient hybrid algorithm is developed based on Sine Cosine Algorithm (SCA) [35] and

Transient Search Optimization (TSO) [36]. The developed approach utilizes an amended version of SCA and then integrates the TSO in a parallel manner to obtain a new algorithm referred to as HSCATSO of better exploration and exploitation phases that result in faster and more reliable optimization results. The developed HSCATSO algorithm was verified with twenty benchmark functions utilizing MATLAB software. Following that, the developed HSCATSO algorithm has been coordinated with a robust MPEA and then used to optimally design the cascaded control schemes parameters of FSPEC in grid-tied PMSG-VSWT in order to enhance wind power production, capability performance and voltage stability. This, in turn, often provides ancillary services to UG operators and retains a stable electricity system. In this context, the MPEA algorithm and the HSCATSO optimization algorithm are coded in a Matlab function file and connected with the PMSG-VSWT system Simulink model for online system optimization and continuous tracking. The contributions of this article are mainly focused on:

- Developing a novel optimization algorithm named hybrid sine cosine algorithm-transient search optimization (HSCATSO) for optimally designing the FSPEC control schemes' parameters of the grid-tied VSWT system.
- Evaluating the efficacy of the developed HSCATSO algorithm by putting it to the test on twenty benchmark functions and statistically comparing the outcomes against those of four well-known algorithms.
- Coordinating between the developed MPEA and HSCATSO optimization algorithm employed in the designing control schemes of the VSWT system to enhance the performance.
- Verifying the effectiveness of the developed control strategies during the scenarios of network severe disturbance and Malaysia's real wind speed profile.

II. CONFIGURATION OF GRID-TIED VSWT SYSTEM

The configuration of the grid-tied VSWT system that was utilised in this study is outlined in this section. As seen in Figure 1, the system is built with a PMSG-VSWT and is tied to the electric power grid by means of an FSPEC and a filter. The FSPEC consists of a GSR, and a GSI linked to one another by a capacitor and excessive voltage protection system. In addition, the FSPEC incorporates three controllers, which can be referred to as the GSI controller, the GSR controller, and the MPEA. In this setup, the PMSG gets mechanical power from the WT shaft and then converts it into electrical power. FSPEC delivers this power to the UG, where it is purified to fit the grid's criteria.

A. WIND TURBINE MODEL

The main driving force of a VSWT is the kinetic energy of the wind which is given by:

$$P_{wind} = 0.5\rho A V_{\omega}^{3} \tag{1}$$

The wind speed (m/s) is represented by V_{ω}, while A denotes the area covered by the wind turbine blades (m^2), and ρ refers to the density of the air (kg/m^3). The Betz limit states that the WT is unable to take advantage of all of the wind's potential energy [37]. Equivalent mechanical power is generated from wind energy using the formula in Equation (2) [38].

$$P_m = 0.5\rho A V_{\omega}^{3} C_p(, \beta) \tag{2}$$

In this context, the power coefficient (C_p) refers to the conversion efficiency. The dynamic behaviour of wind turbines can be described using a general formula for the power coefficient, which is given as follows:

$$C_p(\lambda, \beta) = 0.22(\frac{116}{\lambda_i} - 0.3\beta - 5)e^{\frac{-12.5}{\lambda_i}} \tag{3}$$

With

$$\frac{1}{\lambda_i} = (\frac{1}{\lambda + 0.08\beta} - \frac{0.035}{\beta^3 + 1}) \tag{4}$$

Based on Equation (3), two main factors affect C_P: TSR of the WT blade $\lambda = R\omega_m/V_{\omega}$ and blade angle β. Here ω_m is the angular speed of the rotor and R is the rotor turbine radius. In this study, the pitch angle β is thought to be zero, which is the best value, because this work focuses on the region where the wind speed is less than the nominal speed. Consequently, the C_p is merely reliant on λ [39]. Wind turbines must be turned at an optimal rotational speed ($\omega_{m.opt}$), which results in an optimal power coefficient $C_{p.opt}$ and an optimal TSR, in order to achieve maximum wind power production, regardless of the prevalent wind speed.

B. PMSG MODEL

The PMSG produces electrical energy out of mechanical energy even with the low rotational speed. It has the benefits of an affordable price, decreased copper loss due to the absence of a field winding, and a high electrical power density [40]. In the rotating reference frame (dq-axis), the PMSG supplies the electrical voltages as given by:

$$v_{ds} = R_s i_{ds} + L_d \frac{di_{ds}}{dt} - \omega_e L_q i_{qs} \tag{5}$$

$$v_{qs} = R_s i_{qs} + L_q \frac{di_{qs}}{dt} + \omega_e \psi_f + \omega_e L_d i_{ds} \tag{6}$$

The stator voltages and currents of the PMGS are represented by i_{ds}, i_{qs}, v_{ds}, and v_{qs}, while the stator resistance and inductances are denoted by R_s, L_q, and L_d. The electrical angular speed is represented by ω_e, while the magnetic flux is denoted by ψ_f. Additionally, the electrical angular speed ω_m is associated with the mechanical speed ω_e based on the number of poles in the machine (p_n), and the relationship between the two can be expressed as:

$$\omega_e = P_n \omega_m \tag{7}$$

The expression for the PMSG electromagnetic torque Te is:

$$T_e = \frac{3}{2} P_n[(L_d s - L_q s) i_{ds} i_{qs} - \psi_f i_{qs}] \tag{8}$$

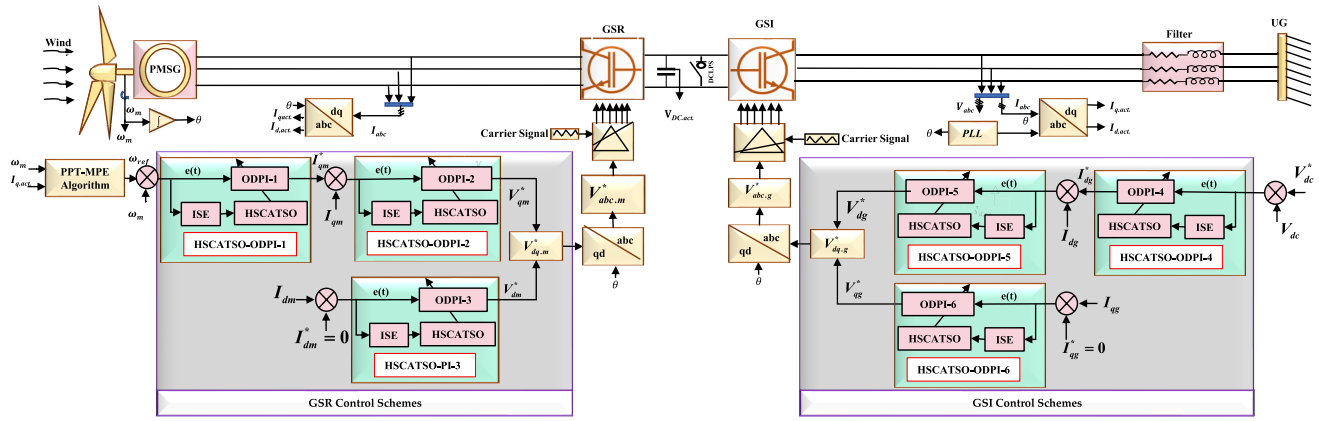

FIGURE 1. Configuration of studied grid-tied VSWT systm.

Hence, the PMSG equation of the dynamic model is formed as Equation (9).

$$J\frac{d\omega_m}{dt} = T_e - T_m - D\omega_m \tag{9}$$

here, T_m, D and J represent the mechanical torque, the generator's rotor damping coefficient and the moment of inertia, respectively.

III. THE FSPEC CONTROL SCHEMES

The amount of kinetic energy that the WT is able to extract from the wind is a nonlinear function with respect to WT's bald spinning speed and wind speed. At a given wind speed, there is a specific spinning speed for each WT that, when reached, captures the maximum amount of power from the wind [41]. As a result, the WT needs to operate at optimal spinning speed in relation to the wind speed. Furthermore, the voltage and frequency generated by the wind are unsuitable for integrating directly with UG [42]. Hence, an FSPEC that has a developed control scheme has been incorporated in order to serve as a connection between the UG terminals and VSWT-PMSG terminals. As shown in Figure 1, the FSPEC utilises three primary control strategies: the GSI, the GSR, and the MPEA. In accordance with the UG framework, the GSI is in charge of controlling the DC-link voltage as well as the terminal current and voltage. The GSR controls the rotor speed based on the MPEA reference speeds to maximise wind power generation [43], whilst the MPEA determines and produces the optimum spinning speed for maximum wind energy harvesting. The following sections elucidate the control schemes implemented on the FSPEC by using the developed HSCATSO and PPT-MPE algorithms-based control system.

A. PPT-MPE ALGORITHM

In WECS, the amount of power extracted from the WT varies in direct proportion to both the turbine's rotational speed and the wind speed. There is only one optimal rotational speed, ω_{m-opt}, for each wind speed that leads to a particular optimal TSR and maximises the amount of wind power. In order to extract the maximum wind power, the wind turbine needs to be set to run in a mode that allows its rotational speed to change depending on the wind speed. Accomplishing this requires incorporating the MPEA with a controlling scheme which in turn seeks the optimal rotational speed ω_{m-opt} and sends information to the GSR controller to alter the WT operates in accordance with the trajectory of MPEA [44]. The ω_{m-opt} of the WT rotor can be calculated for each different wind speed using the conventional MPE method as Equation (10) [45].

$$\omega_{m-opt} = \frac{V_\omega \lambda_{opt}}{R} \tag{10}$$

Using this strategy, determining the optimal rotational speed, denoted by the notation ω_{m-opt}, is straightforward, despite the fact that obtaining an accurate measurement of wind speed can be challenging and costly. The concept of seeking the optimal angular WT rotational speed without considering wind speed measurement is more reliable and promising. Hence, in this study, the focus is on utilizing the sensor-less parabolic prediction technique (PPT) to track maximum power, as it has been demonstrated to be more efficient and effective in [46] compared to other methods.

B. CONTROLLING SCHEMES OF GSR

The main aim of the GSR is to maximize WT's output power and attain the unity power factor at the PMSG terminal guaranteeing optimal operation conditions. To achieve this, an efficient control approach needed to be introduced. In this work, an optimal designed cascaded vector control system is proposed. The control system consists of three control schemes: an outer loop speed controller (ODPI-1) and two inner loop current controllers (ODPI-2 and ODPI-3), as seen in Figure 1. For controlling speed, the PMSG's actual rotor speed (ω_m) is measured and compared to the optimal reference speed (ω_{ref}) provided by MPEA. Then, the difference in speed, known as the speed error ($e(t)$) is inputted into the outer speed ODPI-1 controller to determine the estimated

reference electromagnetic torque, T_e^* as follows:

$$T_e^* = (K_p + \frac{k_i}{S})\left(\omega_{ref} - \omega_m\right) \tag{11}$$

Here the K_i and K_p are the controller parameters that are must be optimally designed, while S represents the magnitude of Laplace. In this domain the obtained T_e^* is consequently used to estimate the desired $q-axis$ stator current (I_{qm}^*) as follows:

$$I_{qm}^* = \frac{T_e^*}{\left(\frac{3}{4}\cdot P\cdot \psi + \frac{3}{4}\cdot P\cdot (L_d - L_q)\cdot i_{ds}\right)} \tag{12}$$

During the inner loop, the estimated value of I_{qm}^* is compared against the actual value of I_{qm} and the resultant error signal is transmitted to the ODPI-2 module. This error signal is utilized to adjust the value of I_{qm} in accordance with the value of I_{qm}^* provided by the ODPI-1 module, with the primary objective being to facilitate the transfer of maximum power to UG. Similarly, the ODPI-3 is applied to fix the d-axis stator current I_{dm} to zero set point I_{dm}^* so as to attain unity power factor operation. The Equations 5 and 6 indicate that stator d and q-axis currents can be controlled by regulating the stator d- and q-axis voltage (V_d^* and V_q^*) respectively and as the following:

$$V_{dm}^* = (K_p + \frac{K_i}{S})\cdot (I_{dm}^* - I_{dm}) \tag{13}$$

$$V_{qm}^* = (K_p + \frac{k_i}{S})\cdot (I_{qm}^* - I_{qm}) \tag{14}$$

The output signal of the ODPI-2 ODPI-3 (V_{dm}^* and V_{qm}^*) are converted to abc frame, $V_{a,b,c}^*$, by means of θ_r that is grasped from the PMSG speed. Subsequently, the $V_{a,b,c}^*$ signals are compared with a 1.65 kHz triangle carrier to produce IGBT switching signals for the GSR system.

C. CONTROLLING SCHEMES OF GSI

The connection of the PMSG-VSWT system to the UG is achieved via a GSI. To ensure meeting the UG requirements, cascaded control schemes based on the ODPIs for GSI are developed. The developed cascaded control schemes are composed of an exterior voltage loop of a slower pace and an inner current loop of a faster pace as shown in Figure 1. The exterior loop controller (ODPI-4) is used to control the DC-link voltage to its set point. While the ODPI-5 and ODPI-6-based interior control loops are used to control the injected active and reactive power via the quadrature and direct currents (I_{dg} and I_{qg}) respectively. In this loop, the I_{dg}^* is retrieved from the exterior loop whereas I_{qg}^* is set to zero, so as to maintain the GSI operates at unity power factor. Afterwards, the ODPI-5's output signal (V_{dg}^*) and ODPI-6's output signal (V_{qg}^*) are transformed into $V_{a,b,c}^*$ signals in the three-phase frame by applying the angle θ_r. The value of θ_r is obtained through a phase-locked-loop scheme. Lastly, the frequency of the carrier signal is compared to the $V_{a,b,c}^*$ signals, resulting in the creation of firing pulses for the IGBT inverter. The equations relevant to the DC-link voltage regulator are given as follows:

$$I_{dg}^* = K_p(V_{dc}^* - V_{dc}) + K_i\int_0^t (V_{dc}^* - V_{dc})dt \tag{15}$$

While the equation for the q-d axis current regulator in relation to the grid $d-$ and $q-$ axis voltage is expressed as follows:

$$V_{qg}^* = I_{qg}^* - K_p(I_{qg}^* - I_{qg}) - K_i\int_0^t (I_{qg}^* - I_{qg})dt \tag{16}$$

$$V_{dg}^* = I_{dg}^* - K_p(I_{dg}^* - I_{dg}) - K_i\int_0^t (I_{dg}^* - I_{dg})dt \tag{17}$$

In the GSI's control structure, V_{dg}^* and V_{dg}^* represent the reference voltage on the $q-d$ axis. The I_{qg}^* and I_{dg}^* are the desired current value on the $q-d$ axis. While the I_{qg} and I_{dg} are the actual measured current on the $q-d$ axis of the grid. The terms K_p and K_i refer to the proportional and integral gains used for controlling the desired variable. These gains are being optimally designed by the proposed HSCATSO optimizer

D. DC-LINK PROTECTING SCHEMES

In the event of a network disruption, the GSI cannot inject the harvested wind energy into the electric power grid due to the abrupt voltage drop along the grid side. The abrupt drop in gride voltage leads to a sudden increase in DC-link voltages as well as uneven power between the grid side and the VSWT system. The DC-link capacitor and the inverter could suffer damage as a result of the excess energy. Therefore, DC-link protecting scheme is needed to protect the system and maintain the DC-Link voltage within acceptable limits, as shown in Figure 1. In this investigation, the DC-link protecting scheme is a protective system coupled with a relay and braking unit [47]. The relay will engage the brake unit whenever the DC link voltage is found to be higher than the permissible limit. Concurrently, the brake unit avoids an over-voltage of the DC-link by routing through swapping the extra power to a resistor, where it is subsequently absorbed as heat.

IV. OPTIMAL DESIGNING MECHANISM

In order to perform online optimal designing of the PI controllers' gains of the control schemes, the HSCATSO optimizer needs to be programmed in a MATLAB function file and reference to the VSWT system Simulink model. In this study, the proposed Simulink model is comprised of six PI controllers (6 integral gains Ki and 6 proportional gains Kp) that are presented in cascaded GSR and GSI controlling system, as depicted in Figure 1. The purpose of the optimal designing process is to achieve optimal design PI controller gains that result in improving the performance of the grid-connected PMSG-VSWT system. In this regard, it is hard to establish the mathematical model of the developed VSWT system due to the fact that it is extremely complex and unpredictable in its behaviour. Moreover, it is nearly

impossible to build a transfer function that precisely captures the relationships between the parameters of the twelve gains and the fitness function. Alternatively, one can develop an index of performance-based controller design relationships that consider the entire closed-loop response pattern. A measure of performance called a performance assessment index can be used to highlight important aspects of a system's response. The summation of ISE is a commonly used metric for evaluating performance, and it was selected as the fitness function for an optimization problem in this particular study. The ISE formula used in this study is presented below:

$$ISE = \int_{o}^{t} (e^2_{\omega_m} + e^2_{iq_m} + e^2_{id_m} + e^2_{V_{dc}} + e^2_{iq_g} + e^2_{id_g})\, dt \quad (18)$$

where e_{ω_m} represents the rotor speed error signals. The e_{id_m} and e_{iq_m} are the i_d and i_q of stator current's error signals, respectively. The $e_{V_{dc}}$ denotes the V_{dc} error signals, whereas e_{id_g} and e_{iq_g} represent the i_d grid and the i_q grid error signals, respectively. The mechanism of optimization begins with proportional gains initialization i.e., the $(K_{p1}, K_{p2}, \ldots, K_{p6})$ and integral gains $(K_{i1}, k_{i2}, \ldots., K_{i6})$ of six PIs that are considered as the controlling variables in the optimization issue. In the optimal design procedure, the PI's gains first values are randomly generated by the HSCATSO optimizer. These values are then constrained to fall within the range [0.5,15] to prevent the optimization process from diverging due to the non-linearities present in the system. Afterwards, the error inputs from all PI controllers are recorded, integrated, squared, and finally combined. Then, the total of the ISE is passed on to the HSCATSO algorithm to be used as the fitness function that requires optimization. The main goal of the optimization task is to reduce the value of the ISE. At each iteration, the grid-connected PMSG-VSWT Simulink model is run, and the HSCATSO looks at the summation of ISE to come up with a new optimized gain for each PI. This optimization process is repeated for a number of preset iterations. Finally, the HSCATSO optimizer assigns the optimal gains that resulted in the lowest ISE into the Simulink model of the VSWT system. Figure 2 shows a flowchart of how the HSCATSO's optimization mechanism works with the VSWT Simulink model to get the optimum gains values.

To verify the effectiveness of the HSCATSO algorithm, optimal design procedures for PI gains of the same model using SCA, GWO, TSO, and PSO have been separately performed. This allowed for a comparison of the different algorithms and the determination of whether the HSCATSO algorithm was the most effective for the specific optimization problem. The detailed optimal design of PI gains of the VSWT system using SCA, GWO, PSO, and TSO and their design principles can be obtained from previous studies in [25] and [33]. However, the design principle of the proposed HSCATSO algorithm has been elucidated in Section IV-A with the aid of a flowchart, pseudo-code, and equations to facilitate a comprehensive and lucid comprehension of its implementation.

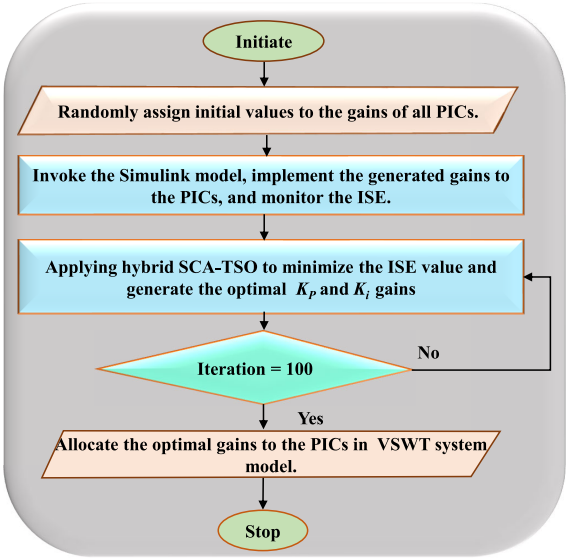

FIGURE 2. Optimization mechanism flowchart.

A. THE PROPOSED HSCATSO ALGORITHM

The design principle of the HSCATSO algorithm is to combine the complementary strengths of the SCA and TSO to achieve a better balance between global and local search and hence improve the overall optimization performance. The SCA is created by Mirjalili in 2016 and utilises the trigonometric functions of sine and cosine for the exploitation and exploration phases in the optimization problem [35]. Although the SCA algorithm can expose an efficient accuracy in comparison with another well-known optimization algorithm, it still may confront the problem of local optima entrapment which is reflected in the computational effort that needs to be overwhelmed. To address the shortcomings of SCA and improve its search functionality, this work is developing a novel hybridizing approach with the TSO [36] and is named the HSCATSO optimization algorithm. The basic idea is to introduce an amended version of SCA and then integrate TSO in a parallel manner to obtain a new hybrid algorithm for better exploitation and exploration phases. The hybridization of SCA with other algorithms has been implemented in previous studies. For instance, Abdulrab et al. [48] hybridised HHO with SCA to enhance further their previous work reported in [49] and [50].

The hierarchical structure of HSCATSO is depicted in Fig. 3, where the SCA search agents in the top layer are responsible for generating individuals that are subsequently updated by TSO in the bottom layer. The bottom layer is organized into M groups, each containing N TSO members. The TSO is initially executed in the bottom layer to update the positions of the individuals. The optimal solution found by each group in the bottom layer is then passed on to the corresponding SCA agent in the top layer. The SCA agents then

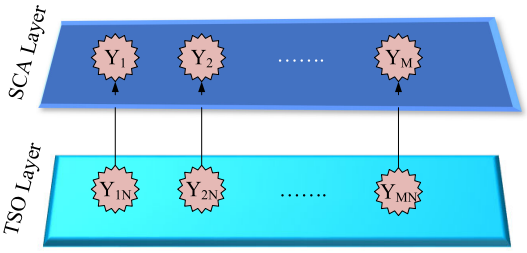

FIGURE 3. The hierarchical form of proposed HSCATSO.

iterate the positions of their associated individuals based on the acquired optimal solutions, resulting in the generation of new equations that represent the exploitation and exploration phases of the search process. The exploration phase of the HSCATSO is mainly controlled by the randomly generated parameter r_4 at the top layer,i.e, r_4<0.5, and performed by the arithmetic equation 19.

$$Y_{t+1}^{i} = \begin{cases} Y_t^* + \left(y_t - C_1 * Y_t^*\right)e^{-X} + r_1 \sin\left(r_2\right) \times \left|r_3 P_i^t - \right. \\ \left.\left(Y_t^* + \left(y_t - C_1 * Y_t^*\right)e^{-X}\right)\right|, \quad r_5 < 0.5 \\ Y_t^* + e^{-X}\left[\cos\left(2\pi X\right) + \sin\left(2\pi X\right)\right]\left|y_t - C_1 * Y_t^*\right| \\ + r_1 \sin\left(r_2\right) \times \left|r_3 P_i^t - \left(Y_t^* + e^{-X}\left[\cos\left(2\pi X\right) + \right.\right.\right. \\ \left.\left.\left.\sin\left(2\pi X\right)\right]\left|y_t - C_1 * Y_t^*\right|\right)\right|, \quad r_5 \geq 0.5 \end{cases} \tag{19}$$

where position of the t-th individual in the SCA layer corresponding to the i-th search agent in the TSO layer is described by Y_{t+1}^{i}, while y_t denotes the position of the t-th search agent in the SCA layer. The best updated solution is represented by $Y_t^* = p_i^t$. Randomly generated parameters, r_5 and r_6, play a crucial role in the proposed HSCATSO by determining the balance between exploitation and exploration in the TSO layer. Specifically, r_5 is responsible for switching between exploitation and exploration. Other definitions of the parameters are given as:

$$\begin{aligned} Y_t^* &= P_i^t \\ r_1 &= 2 - t\frac{2}{T} \\ r_2 &= 2\pi * rand\ () \\ r_3 &= 2 * rand\ () \\ X &= 2 * r_1 * r_6 - r_1 \\ C_1 &= K * r_1 * r_6 + 1 \end{aligned} \tag{20}$$

The exploitation phase, on the other hand, is performed by the following arithmetic equation when $r_4 \geq 0.5$:

$$Y_{t+1}^{i} = \begin{cases} Y_t^* + \left(y_t - C_1 * Y_t^*\right)e^{-X} + r_1 \cos\left(r_2\right) \times \left|r_3 P_i^t - \right. \\ \left.\left(Y_t^* + \left(y_t - C_1 * Y_t^*\right)e^{-X}\right)\right|, \quad r_5 < 0.5 \\ Y_t^* + e^{-X}\left[\tan\left(2\pi X\right) + \sin\left(2\pi X\right)\right]\left|y_t - C_1 * Y_t^*\right| \\ + r_1 \cos\left(r_2\right) \times \left|r_3 P_i^t - \left(Y_t^* + e^{-X}\left[\tan\left(2\pi X\right) + \right.\right.\right. \\ \left.\left.\left.\sin\left(2\pi X\right)\right]\left|y_t - C_1 * Y_t^*\right|\right)\right|, \quad r_5 \geq 0.5 \end{cases} \tag{21}$$

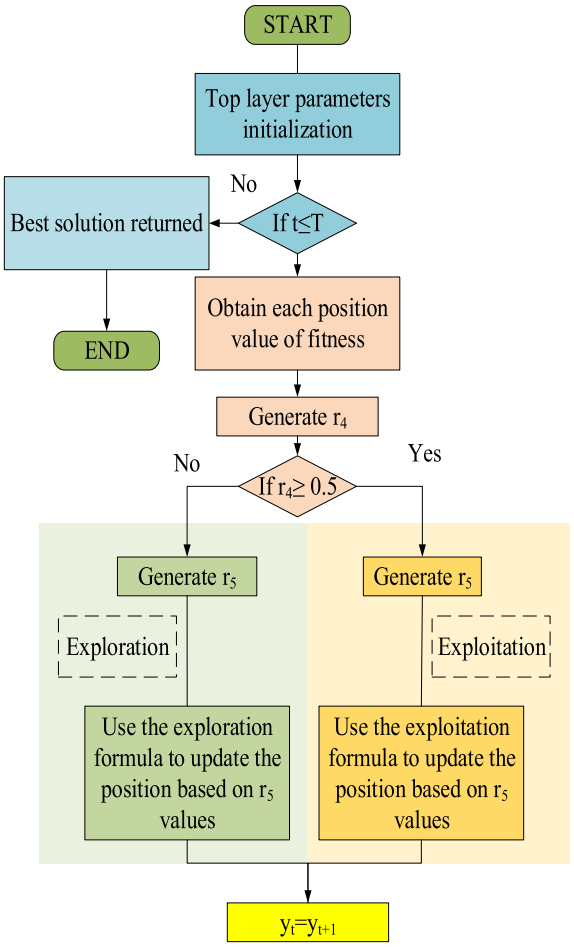

FIGURE 4. The flowchart of the proposed HSCATSO.

TABLE 2. List of HSCATSO conditions and various operational phases.

Phase category	Top layer condition	Bottom layer condition	Related Expression
Exploration	r_4<0.5	r_5<0.5	Exploitation at the bottom layer Case 1 of (19)
		r_5>=0.5	Exploration at the bottom layer Case 2 of (19)
Exploitation	r_4>=0.5	r_5<0.5	Exploitation at the bottom layer Case 1 of (21)
		r_5>=0.5	Exploration at the bottom layer Case 2 of (21)

B. PSEUDO-CODE OF HSCATSO ALGORITHM

The HSCATSO approach involves distinct exploration and exploitation phases in the SCA layer at the top. The TSO layer at the bottom plays a crucial role in updating the current location during each iteration of the optimization process. Table 2 describes the conditions that dictate when the system should switch between the exploration and exploitation phases. Figure 4 reveals the implementation flowchart of the HSCATSO algorithm.

Furthermore, a pseudo-code has been developed for the HSCATSO, which is designed to be easy to understand.

Algorithm 1 HSCATSO

Input:

- Set the upper bound and lower bound of Y solutions between $15 \leq k_p$ and $k_i \leq 0.5$.
- Set the population size of N
- Initiate the gains of the PIs in a random manner. $\{kp_1,\ kp_2 \ldots kp_6\}$ & $\{ki_1,\ ki_2 \ldots ki_6\}$
- Set Maximum iterations T

Output:

- The best-selected solution (Y^*) for PIs gain values

Loop Process

while ($t \leq$ *Max iterations* T) **do**
  Calculate fitness function (ISE)
  Define the best-selected solution (Y^*)
  Update r_1, r_2, r_3,, r_4 and r_5
  Exploration phase
  Top Layer Condition
  if R_4<0.5 **then**
    Bottom Layer Condition
    if r_5 <0.5 **then**
      Update agents' positions in the search space with Case 1 of (19)
    else
      Update agents' positions in the search space with Case 2 of (19)
    end if
    Exploitation phase
    Top Layer Condition
  else
    Bottom Layer Condition
    if r_5 <0.5 **then**
      Update agents' positions in the search space with Case 1 of (21)
    else
      Update agents' positions in the search space with Case 2 of (21)
    end if
  end if
  $t = t + 1$
end while
Return (Y^*) **for PIC gain values**
Record the best-obtained values for the gains of PICs
Assign the best-obtained values to the VSWT Simulink model

Algorithm 1 outlines the basic principles of the HSCATSO algorithm with respect to PIs gains optimization issue.

C. VERIFICATION OF THE PROPOSED HSCATSO

In the domain of optimization utilizing meta-heuristic algorithms, multiple test cases must be used to verify an algorithm's effectiveness. In this regard, the robustness of the proposed HSCATSO optimization algorithm is verified by utilizing 20 recognized benchmark functions. Figure 5 show the surface plots of the considered benchmark functions. The benchmark functions are divided into three groups: uni-modal functions, multi-modal functions, and hybrid functions, as illustrated in Tables 3, 4 and 5 respectively. The functions of uni-modal are typically employed to evaluate the exploitation capability of an algorithm, while multi-modal are typically utilised to assess its exploration capability. The verification trials of the proposed algorithm have been run using MATLAB R2022a on a PC Intel(R) Core(TM) i5-8250U CPU @3.40 GHz (8 CPUs), 12 GB, Windows 11-64 bits).

The results and performance of the proposed HSCATSO have been compared with well-established optimization algorithms which are widely applied in different engineering problems such as SCA, GWO, PSO and TSO. The comparison and evaluation are performed based on mean, best, worst, and standard deviation (STD). For a fair comparison, all algorithms have the same population size of 30, iterations number of 300 and run a number of 30. The statistical analysis outcomes including the worst, best, mean and standard deviation of 30 separated runs for all algorithms are gathered and compared. Table 6 shows only the statistical analysis and rank of algorithms for **F-1**, however, the algorithm's rank for all functions **(F-1 to F-20)** is displayed in Figure 7. The comparison of the data showed that the HSCATSO algorithm outperformed other algorithms in terms of the number of best mean values (14/20) obtained. Thus, it ranks first among other algorithms, whereas SCA achieved second place. Moreover, Figure 6 demonstrated that the developed HSCATSO optimization algorithm converges significantly faster than the SCA, TSO, GWO and PSO algorithms.

D. OPTIMAL DESIGNING RESULTS

The optimization procedure is carried out for the simulated VSWT system model shown in Figure 1. During the online optimization process, the proposed and compared algorithms have been employed to diminish the fitness function (ISE) in a parallel way in order to convey the optimal PI's gains. The optimization's iteration number is set to 100 and the duration of each iteration in the simulation has been configured to 5 seconds. The optimization outcomes confidently confirm that the HSCATSO optimization algorithm generated the best ODPI gains, leading to the best ISE (lowest error) compared to the other tested algorithm. The optimal gain values of the ODPI controllers and the best fitness function **(Best ISE)** obtained by all algorithms are listed in Table 7. Moreover, the convergence speed curve of the fitness function for all algorithms during 100 iterations is illustrated in Figure 8. The results in the figure demonstrated that the HSCATSO algorithm achieves faster convergence at minimizing ISE compared to the SCA, TSO, GWO, and PSO algorithms.

TABLE 3. Benchmark of uni-modal functions.

Func.	Range	Description
Benchmark of Uni-modal functions		
F-1	[-100,100]	$F(\mathbf{x}) = \sum_{i=1}^{n} x_i^2$
F-2	[-10,10]	$F(\mathbf{x}) = \sum_{i=0}^{n} \lvert x_i \rvert + \prod_{i=0}^{n} \lvert x_i \rvert$
F-3	[-100,100]	$F(\mathbf{x}) = \sum_{i=1}^{d} \left(\sum_{j=1}^{i} x_j \right)^2$
F-4	[-100,100]	$F(\mathbf{x}) = \sum_{i=1}^{n} \left([x_i + 0.5] \right)^2$

TABLE 4. Benchmark of multi-modal functions.

Func.	Range	Description
F-5	[-128,128]	$F(\mathbf{x}) = \sum_{i=0}^{n} i x_i^4 + \text{random}(0,1)$
Fun-6	[-500,500]	$F(\mathbf{x}) = \sum_{i=1}^{n} \left(-x_i \sin\left(\sqrt{\lvert x_i \rvert} \right) \right)$
F-7	[-32,32]	$F(\mathbf{x}) = -20 \exp\left(-0.2 \sqrt{\frac{1}{n} \sum_{i=1}^{n} x_i^2} \right) - \exp\left(\frac{1}{n} \sum_{i=1}^{n} \cos(2\pi x_i) \right) + 20 + e$
F-8	[-50,50]	$F(\mathbf{x}) = \frac{\pi}{n} \left\{ 10 \sin(\pi y_1) \right\} + \sum_{i=1}^{n-1} (y_i - 1)^2 \left[1 + 10 \sin^2(\pi y_{i+1}) \right] + \sum_{i=1}^{n} u(x_i, 10, 100, 4) \Big]$, where, $y_i = 1 + \frac{x_i + 1}{4}$, $u(x_i, a, k, m) \begin{cases} K(x_i - a)^m & \text{if } x_i > a \\ 0 & -a \le x_i \ge a \\ K(-x_i - a)^m & -a \le x_i \end{cases}$
F-9	[-65,65]	$F(\mathbf{x}) = \left(\frac{1}{500} + \sum_{j=1}^{25} \frac{1}{j + \sum_{i=1}^{2}} (x_i - a_{ij}) \right)^{-1}$
Fun-10	[-5,5]	$F(\mathbf{x}) = \sum_{i=1}^{11} \left[a_i - \frac{x_1 (b_i^2 + b_i x_2)}{b_i^2 + b_i x_3 + x_4} \right]^2$
F-11	[0,1]	$F(\mathbf{x}) = -\sum_{i=1}^{4} c_i \exp\left(-\sum_{i=1}^{6} a_{ij} (x_j - p_{ij})^2 \right)$
F-12	[0,1]	$F(\mathbf{x}) = -\sum_{i=1}^{5} \left[(X - a_i)(X - a_i)^T + c_i \right]^{-1}$

TABLE 5. Benchmark of hybrid functions.

Func.	Range	Description
F-13	[-512,512]	$F(\mathbf{x}) = -(x_2 + 47) \sin\left(\sqrt{\lvert x_2 + \frac{x_1}{2} + 47 \rvert} \right) - x_1 \sin\left(\sqrt{\lvert x_1 - (x_2 + 47) \rvert} \right)$
F-14	[-10,10]	$F(\mathbf{x}) = -\left\lvert \sin(x_1) \cos(x_2) \exp\left(\left\lvert 1 - \frac{\sqrt{x_1^2 + x_2^2}}{\pi} \right\rvert \right) \right\rvert$
F-15	[-5.12,5.12]	$F(\mathbf{x}) = \left(\sum_{i=1}^{5} i \cos((i+1)x_1 + i) \right) \left(\sum_{i=1}^{5} i \cos((i+1)x_2 + i) \right)$
F-16	[-100,100]	$F(\mathbf{x}) = -\cos(x_1) \cos(x_2) \exp\left(-(x_1 - \pi)^2 - (x_2 - \pi)^2 \right)$
F-17	[-2,2]	$F(\mathbf{x}) = [1 + (x_1 + x_2 + 1)^2 (19 - 14x_1 + 3x_1^2 - 14x_2 + 6x_1 x_2 + 3x_2^2)] \times [30 + (2x_1 - 3x_2)^2 (18 - 32x_1 + 12x_1^2 + 48x_2 - 36x_1 x_2 + 27x_2^2)]$
Fun-18	[0,10]	$F(\mathbf{x}) = -\sum_{i=1}^{m} \left(\sum_{j=1}^{4} (x_j - C_{ji})^2 + \beta_i \right)^{-1}$, where, $m = 10$; $\beta = \frac{1}{10}(1,2,2,4,4,6,3,7,5,5)^T$, $\mathbf{C} = \begin{pmatrix} 4.0 & 1.0 & 8.0 & 6.0 & 3.0 & 2.0 & 5.0 & 8.0 & 6.0 & 7.0 \\ 4.0 & 1.0 & 8.0 & 6.0 & 7.0 & 9.0 & 3.0 & 1.0 & 2.0 & 3.6 \\ 4.0 & 1.0 & 8.0 & 6.0 & 3.0 & 2.0 & 5.0 & 8.0 & 6.0 & 7.0 \\ 4.0 & 1.0 & 8.0 & 6.0 & 7.0 & 9.0 & 3.0 & 1.0 & 2.0 & 3.6 \end{pmatrix}$
F-19		$F(\mathbf{x}) = -\sum_{i=1}^{4} \alpha_i \exp\left(-\sum_{j=1}^{6} A_{ij} (x_j - P_{ij})^2 \right)$, where, $\alpha = (1.0, 1.2, 3.0, 3.2)^T$, $\mathbf{A} = \begin{pmatrix} 10 & 3 & 17 & 3.50 & 1.7 & 8 \\ 0.05 & 10 & 17 & 0.1 & 8 & 14 \\ 3 & 3.5 & 1.7 & 10 & 17 & 8 \\ 17 & 8 & 0.05 & 10 & 0.1 & 14 \end{pmatrix}$, $\mathbf{P} = 10^{-4} \begin{pmatrix} 1312 & 1696 & 5569 & 124 & 8283 & 5886 \\ 2329 & 4135 & 8307 & 3736 & 1004 & 9991 \\ 2348 & 1451 & 3522 & 2883 & 3047 & 6650 \\ 4047 & 8828 & 8732 & 5743 & 1091 & 381 \end{pmatrix}$
F-20	[0,π]	$F(\mathbf{x}) = -\sum_{i=1}^{d} \sin(x_i) \sin^{2m}\left(\frac{i x_i^2}{\pi} \right)$

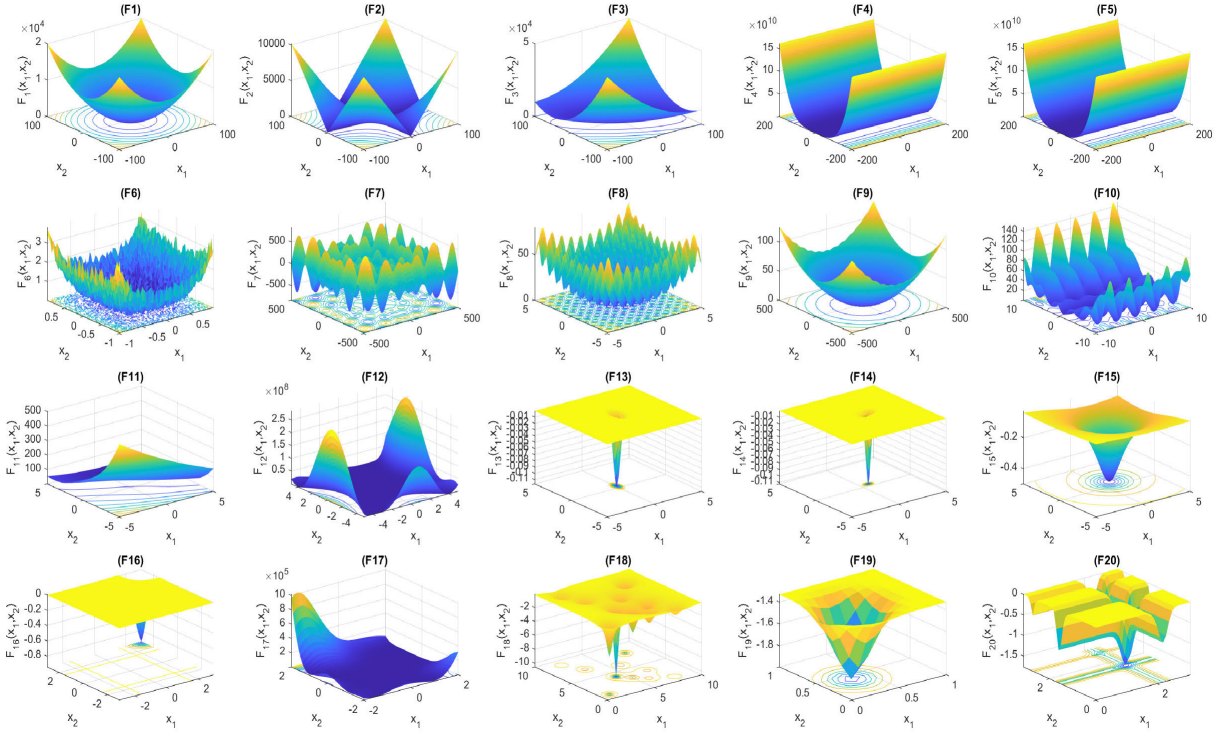

FIGURE 5. Search space plots of the benchmark functions.

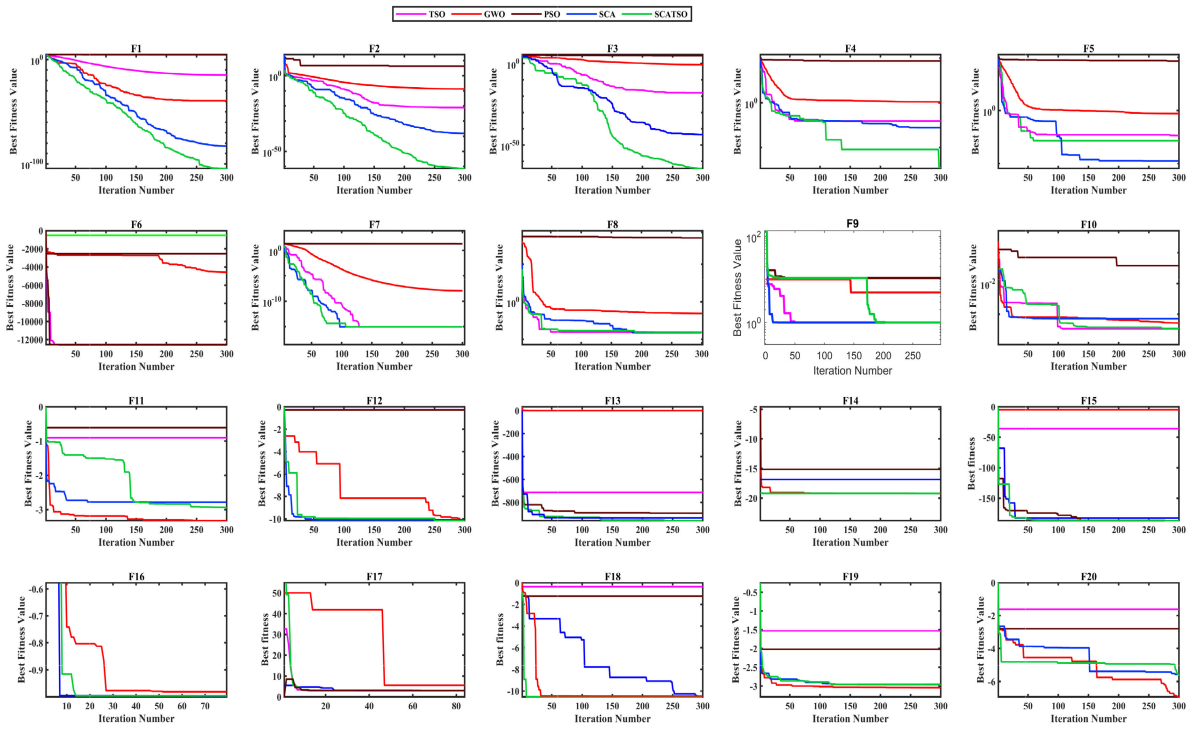

FIGURE 6. Convergence output of the considered benchmark functions.

TABLE 6. Statistical analysis of F-1 and algorithms rank.

Function	GM	STAT	HSCATSO	TSO	GWO	SCA	PSO
F-1	0	Mean	2.2883E-175	7.4136E-66	5.8087E-66	3.3014E-111	4.4909E+04
		Best	3.7137E-212	1.0899E-84	8.6559E-72	3.5499E-134	3.6733E+04
		Worst	2.2850E-174	7.4136E-65	5.6674E-65	3.2646E-110	5.3865E+04
		STD	0.0000E+00	2.3444E-65	1.7874E-65	1.0311E-110	6.7386E+03
		Rank	1	4	3	2	5
Mean of Rank			1.3515	2.4404	3.0763	2.1496	3.7053
Final Ranking			1	3	4	2	5

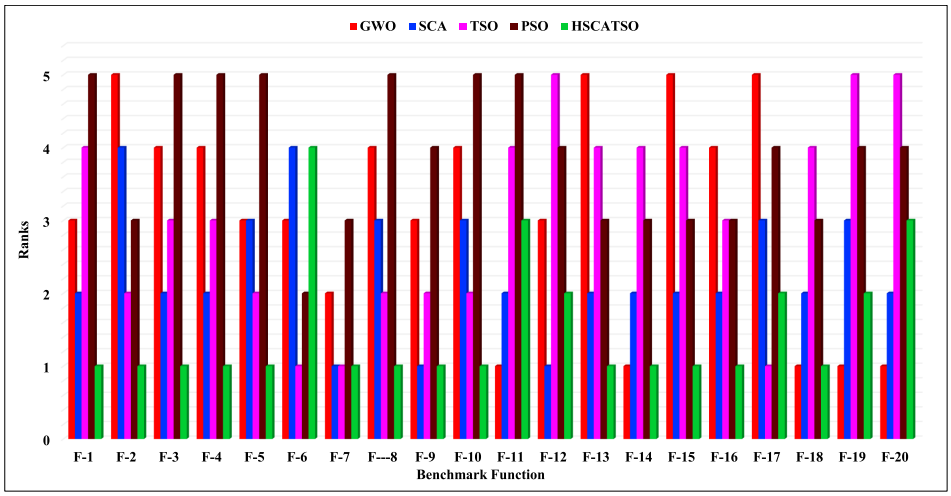

FIGURE 7. Friedman rank of optimization algorithm for 20 benchmark function.

TABLE 7. ODPIs gains and Best ISEs.

c	ODPI-1		ODPI-2		ODPI-3		ODPI-4		ODPI-5		ODPI-6		Best ISE
	Ki-1	Kp-1	Ki-2	Kp-2	Ki-3	Kp-3	Ki-4	Kp-4	Ki-5	Kp-5	Ki-6	Kp-6	
HSCATSO	12.600	12.600	12.600	1.620	12.600	12.600	1.621	12.600	1.621	10.999	1.861	12.600	**0.1106**
SCA	15.000	15.000	3.659	15.000	4.938	15.000	3.759	15.000	3.318	15.000	2.050	15.000	**0.1407**
TSO	6.541	5.282	9.758	12.362	11.895	11.520	2.626	4.045	1.760	10.401	4.086	12.362	**0.1690**
GWO	10.937	10.769	10.866	10.606	9.062	5.757	4.205	8.009	4.569	5.816	2.756	6.857	**0.1772**
PSO	7.810	13.865	10.512	7.461	8.725	14.609	11.754	13.432	8.703	3.092	8.703	3.092	**0.2093**

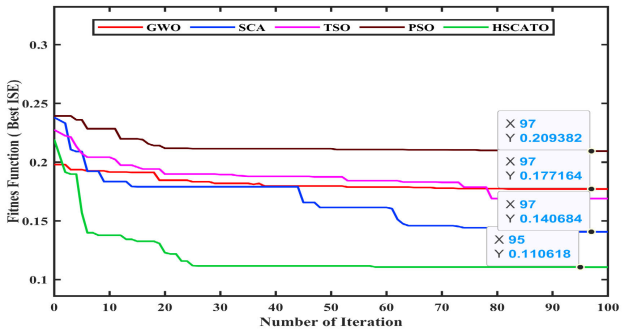

FIGURE 8. Algorithms' fitness function convergence.

V. SIMULATION ANALYSIS AND DISCUSSION

The detailed model of the grid-tied VSWT system shown in Figure 1 is modelled and simulated in MATLAB/Simulink to evaluate the performances of the developed HSCATSO-based ODPIs control schemes. The performance evaluation has been done under real wind speed data and grid disturbance circumstances so as to establish the validity of the grid-tied VSWT system model and the effectiveness of the developed control schemes. Furthermore, the simulation outcomes of the HSCATSO-based ODPIs control schemes are compared with that achieved using the SCA, TSO, GWO, and PSO-based ODPIs control schemes. The VSWT system's simulation parameters of this investigation are outlined in [33].

A. EVALUATION UNDER REAL WIND SPEED PROFILE

Wind speed variations pose a significant challenge for control schemes of the VSWT system. To represent and predict the performance of the developed HSCATSO-based ODPIs control schemes in factual environmental circumstances, real wind speed data displayed in Figure 9 is utilised. The data was taken from NASA's Power Project for the location of a Latitude of 7.1453, and a Longitude of 116.4448 at Kudat, Sabah,

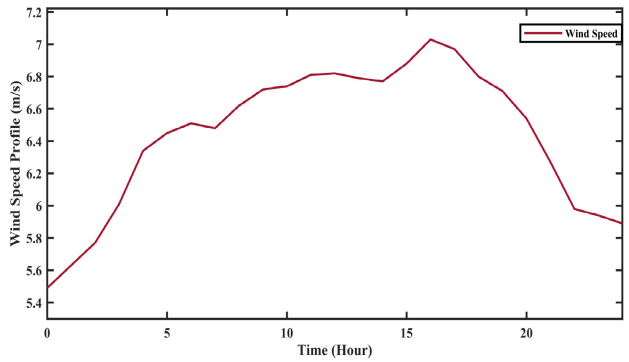

FIGURE 9. Real wind speed profile.

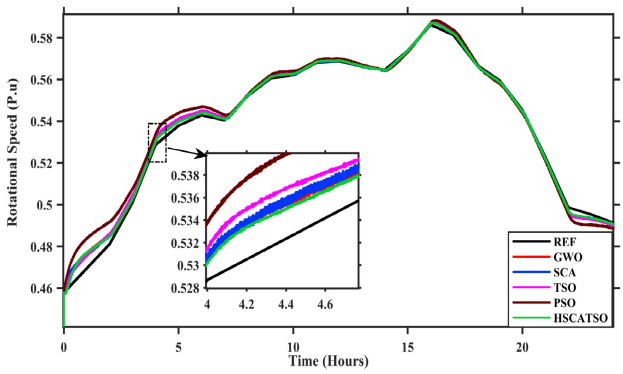

FIGURE 10. WT rotational speed.

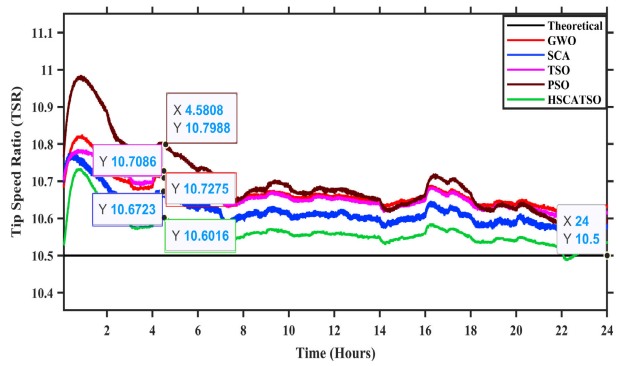

FIGURE 11. Tip speed ratio response.

Malaysia for one day (05 Jan 2022) at one-hour intervals [51]. Meanwhile, the response of the most important system parameters such as rotational speed regulation, tip speed ratio, power coefficient (Cp) and extracted wind power have been analyzed, evaluated, and compared to that obtained using the other four control schemes.

The simulation results displayed in Figure 10 demonstrated that the ODPIs control schemes designed by HSCATSO outperformed all compared ODPIs control schemes in terms of retaining PMSG rotating speed at its optimal value in response to changes in wind speed. Moreover, Figure 11 pointed out the response of the system's TSR and assured that the ODPIs control scheme based on the HSCATSO has succeeded in keeping the TSR closer to the optimal value (10.5) better than the ODPIs control schemes designed by

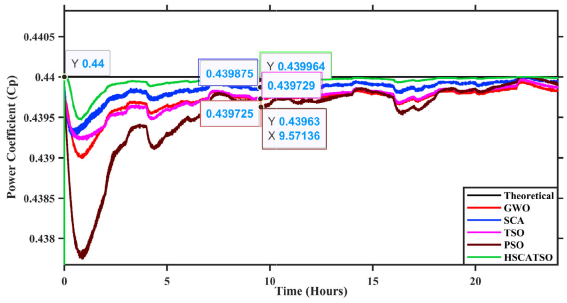

FIGURE 12. Power Coefficient response.

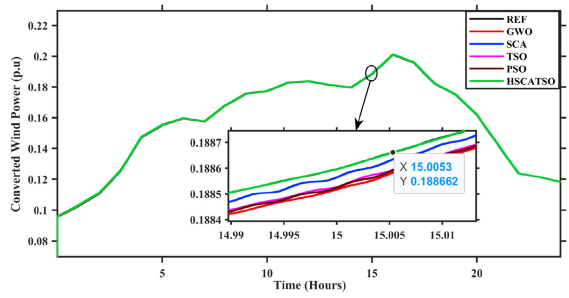

FIGURE 13. Extracted wind power.

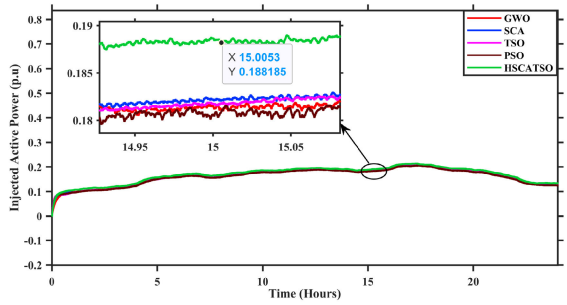

FIGURE 14. Injected active power into UG.

others algorithms. This instantly reflects on the Cp response as emerges in Figure 12 which affirmed that the developed ODPIs control schemes created by HSCATSO surpassed the other ODPIs control schemes at maintaining the system operating nearly at optimal Cp (0.44) regardless of wind speed changes. In view of extracted wind power, Figure 13 proved that the VSWT system using the developed HSCATSO-based ODPIs scheme was able to harness more wind energy than that using the compared ODPIs schemes.

To further verify the superior performance of the developed HSCATSO-based ODPIs control schemes under real wind speed profiles, the significant parameters of the power system, including the injected active power, injected reactive power, DC-link voltage and terminal voltage have been assessed, analysed and compared to those obtained using the competitive control schemes. Figure 14 confirms that when ODPIs designed by HSCATSO are utilized, the injected active power into the utility grid is more exact and more intimate to the rated value than when using the ODPIs designed by TSO, GWO, and PSO. Besides, Figure 15 also confirms that the HSCATSO-based ODPIs control system has more

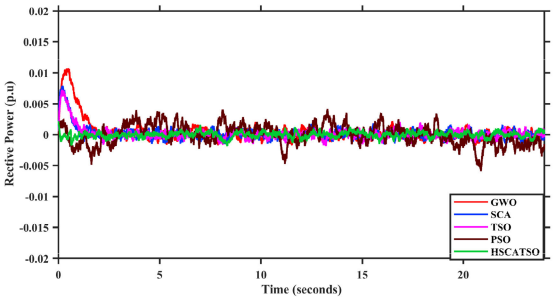

FIGURE 15. Injected reactive power into UG.

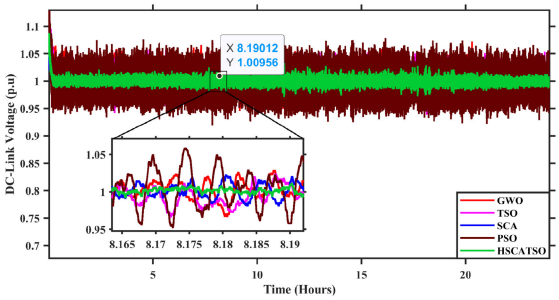

FIGURE 16. DC-link voltage response at varied wind speed.

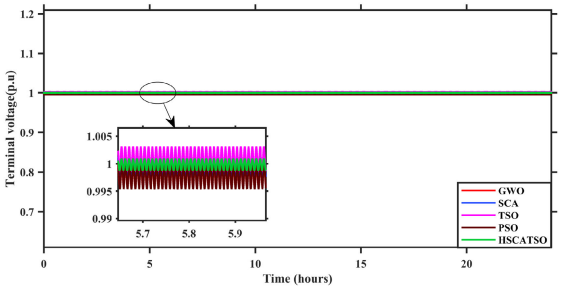

FIGURE 17. Terminal voltage under wind speed variation.

capability and robustness of adjusting the injected reactive power to zero with a lower ripple and better damped as compared to other ODPIs control systems.

The magnified views in Figure 16 elucidate the Dc-link voltage response and assure that using ODPIs designed by HSCATSO resulted in a perfect regulation for the DC-link voltage with the lowest ripple as compared to the other four ODPIs control schemes despite wind speed variations. Figure 17 illustrates Line voltage response. The enlarged visions clearly assert that the developed ODPIs control scheme designed via HSCATSO scheme has accurately realised the terminal voltage rated value with fewer oscillations as compared to the ODPIs control scheme designed by the other benchmark control schemes. This in turn can be considered a good ancillary service in terms of maintaining grid voltage stability. The performance evaluation under variation of wind speed profile obviously indicated that the high response, accuracy, and merit of the developed HSCATSO-based ODPIs control scheme reflect the meticulous design and its robustness to diminish the error signals, achieving rigorous and adequate responses compared with the four mentioned control schemes.

B. EVALUATION UNDER DISTURBANCE CONDITION

This part analyses and evaluates the system response during a network disturbance that results in a terminal voltage drop. The evaluation aims to assess the efficacy of the HSCATSO-based ODPIs control scheme in enhancing the transient stability response of the grid-tied VSWT system. In the simulation, it is imitated a transient drop in the grid's terminal voltage of 75% occurred at the time =3 second for the duration of 0.4 seconds. The wind speed is set to stay steady at 5 m/s because the transient condition is very short.

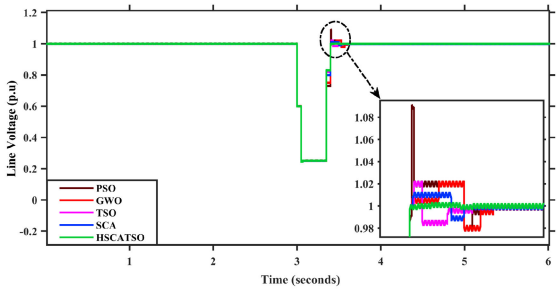

FIGURE 18. Line voltage response under transient event.

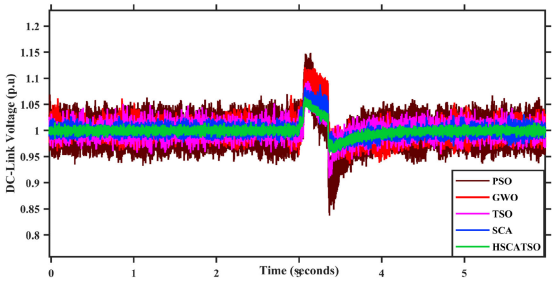

FIGURE 19. Dc-link voltage response under transient event.

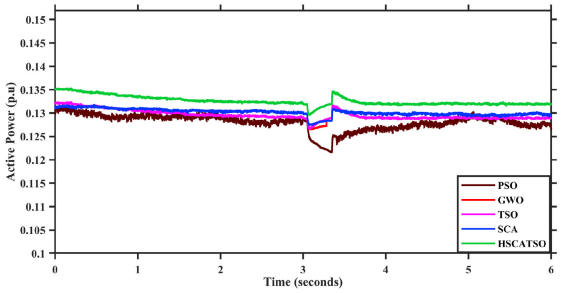

FIGURE 20. Active power response under transient event.

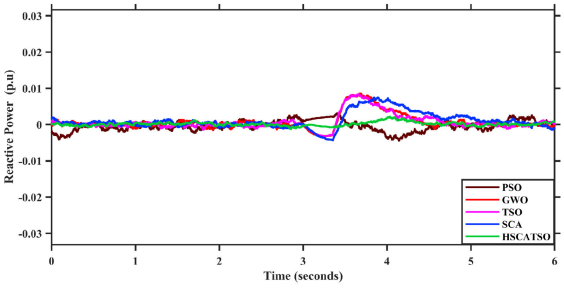

FIGURE 21. Reactive power response under transient event.

TABLE 8. Transient behaviour details.

System Response	Specification	PSO	GWO	TSO	SCA	HSCATSO
Line Voltage Response	Percent Overshoot (%)	9.1	2.0	2.0	1.5	0.17
	Steady-State Error (pu)	0.004	0.0034	0.003	0.0028	0.0012
DC-Link Voltage Response	Percent Overshoot (%)	14.8	11.7	9.4	8.6	6.4
	Percent Undershoot(%)	16.3	6.2	9.1	4.9	2.8
Active Power Response	Steady-State Error (pu)	0.005	0.0021	0.0029	0.0019	0.0002
	Percent Undershoot (%)	8.3	4.45	3.87	3.41	1.18
Reactive Power Response	Steady-State Error(pu)	0.003	0.0015	0.001	0.0012	0.0001
	Percent Overshoot(%)	0.33	0.85	0.82	0.75	0.21

In the event of a voltage drop, an overcurrent relay would sense the increased current and set off the circuit breaker. Simultaneously the GSI controller injects reactive power into the system as an auxiliary service to voltage dip compensation in order to sustain network stability. Then the circuit breaker is re-closed and the grid voltage returned to the pre-dip value of 1 p.u, as illustrated in Figure 18. The response of the ODPIs control schemes optimized with the developed HSCATSO at the transient condition has been compared with the ODPIs control schemes optimized by SCA, TSO, GWO, and PSO. The results demonstrated that the voltage terminal response utilizing the HSCATSO-based ODPIs strategy was better damped and had a lower peak overshoot than that of using the ODPIs control schemes optimized by the other four algorithms. In such conditions, the dropping of the voltage terminal leads to the DC-link voltage increasing due to a reduction in grid active power, whilst the yielded active power from the PMSG keeps constant. The rapid upsurge of the DC-link voltage at the instant of a terminal voltage dip causes unstable operation and may damage the FSPEC as well as the DC-link capacitor. In order to preserve the DC-link voltage responsiveness within an allowable threshold during a dropping voltage situation, the DC-link protection system with a braking unit and overvoltage relay was included in the introduced control scheme. Figure 19 ascertained that the proposed HSCATSO-based ODPI approach accomplished a much faster response, lower overshoot, and less ripple in the DC-link Voltage compared to the other four algorithm-based ODPIs control schemes. The responses of active power and reactive power during the voltage sag are illustrated in Figure 20 and Figure 21 respectively. It can be seen that during the voltage dip, the active deteriorates and consequently the reactive power increases in order to bring the system back to its healthy condition. The simulation results shown in Figure 20 indicated that using ODPIs managed by HSCATSO resulted in a lower active power deterioration, faster recovery, and higher injected power into the utility grid compared to the ODPIs control schemes handled by SCA, TSO, GWO and PSO algorithm. Moreover, Figure 21 confirmed that the reactive power compensation for voltage recovery assistance is the lowest value and the most enriched in comparison with that achieved by the other ODPIs control schemes. Table 8 furnishes an exhaustive description of the system's transient response characteristics, encompassing essential performance metrics including, percent undershoot, percent overshoot and steady-state error for the fives algorithms being studied. Notably, the ODPIs control designed via the HSCATSO scheme is more effective in diminishing the system's overshoot, undershoot, steady state error, and oscillation compared to the ODPIs managed by the other algorithms. According to the transient response outcomes, it is fair to assert that the ODPIs being designed via the proposed HSCATSO scheme are considered as a reliable and effective means for providing auxiliary services and enhancing the transient performance of the VSWT system.

VI. CONCLUSION

This work has introduced a novel hybrid approach labelled as HSCATSO of better exploration and exploitation phases for optimal designing the parameters of FSPEC control schemes interfacing the grid-tied VSWT system in coordination with a robust MPEA. The main objective of the optimal designing and coordination procedure was to form enhanced control schemes for achieving the best wind harvesting and improving the performance of the VSWT system under dynamic and transient operating circumstances. With regard to this, the HSCATSO picks the optimal parameters of control schemes based on the minimum ISE summation of system variables. The feasibility of the developed HSCATSO is verified by utilising twenty benchmark functions and statistical analysis against four well-known algorithms. The performance of the developed ODPIs control schemes being designed by HSCATSO has been evaluated under grid disturbance as well as real wind speed conditions and the response has been compared with that achieved using four competitive ODPI control schemes. The statistical analysis verified that the HSCATSO algorithm outperformed other algorithms at solving an optimization problem with faster convergence speed. Moreover, the simulation outcomes affirmed that the ODPIs control schemes designed by the HSCATSO and coordinated with MPEA resulted in higher power harvesting and enhanced the grid-tied VSWT system stability better than the ODPIs control schemes handled by the other four algorithms.

REFERENCES

[1] Y. Zhang, J. Wei, Q. Gao, X. Shi, and D. Zhou, "Coordination between the energy-consumption permit trading scheme and carbon emissions trading: Evidence from China," *Energy Econ.*, vol. 116, Dec. 2022, Art. no. 106433.

[2] Q. Jiang, Z. U. Rahman, X. Zhang, and M. S. Islam, "An assessment of the effect of green innovation, income, and energy use on consumption-based CO_2 emissions: Empirical evidence from emerging nations BRICS," *J. Cleaner Prod.*, vol. 365, Sep. 2022, Art. no. 132636.

[3] Global Wind Energy Council. *Global Wind Report 2021*. Accessed: Oct. 11, 2022. [Online]. Available: https://gwec.net/global-wind-report-2021/

[4] Statista. *Projected Global Cumulative Wind Power Capacity From 2017 to 2022*. Accessed: Oct. 19, 2022. [Online]. Available: https://www.statista.com/statistics/185551/global-wind-market-forecast-by-cumulative-capacity-since-2010/
[5] D. Bogdanov, M. Ram, A. Aghahosseini, A. Gulagi, A. S. Oyewo, M. Child, U. Caldera, K. Sadovskaia, J. Farfan, L. D. S. N. Barbosa, M. Fasihi, S. Khalili, T. Traber, and C. Breyer, "Low-cost renewable electricity as the key driver of the global energy transition towards sustainability," *Energy*, vol. 227, Jul. 2021, Art. no. 120467.
[6] K. Koiwa, Y. Li, K.-Z. Liu, T. Zanma, and J. Tamura, "Full converter control for variable-speed wind turbines without integral controller or PLL," *IEEE Trans. Ind. Electron.*, vol. 67, no. 11, pp. 9418–9428, Nov. 2020.
[7] X. Zeng, T. Liu, S. Wang, Y. Dong, and Z. Chen, "Comprehensive coordinated control strategy of PMSG-based wind turbine for providing frequency regulation services," *IEEE Access*, vol. 7, pp. 63944–63953, 2019.
[8] R. Basak, G. Bhuvaneswari, and R. R. Pillai, "Low-voltage ride-through of a synchronous generator-based variable speed grid-interfaced wind energy conversion system," *IEEE Trans. Ind. Appl.*, vol. 56, no. 1, pp. 752–762, Jan. 2020.
[9] D. Reddy and S. Ramasamy, "Design of RBFN controller based boost type Vienna rectifier for grid-tied wind energy conversion system," *IEEE Access*, vol. 6, pp. 3167–3175, 2018.
[10] S. M. Tripathi, A. N. Tiwari, and D. Singh, "Grid-integrated permanent magnet synchronous generator based wind energy conversion systems: A technology review," *Renew. Sustain. Energy Rev.*, vol. 51, pp. 1288–1305, Nov. 2015.
[11] V. Yaramasu, A. Dekka, M. J. Durán, S. Kouro, and B. Wu, "PMSG-based wind energy conversion systems: Survey on power converters and controls," *IET Electr. Power Appl.*, vol. 11, no. 6, pp. 956–968, 2017.
[12] Y. Mousavi, G. Bevan, I. B. Kucukdemiral, and A. Fekih, "Sliding mode control of wind energy conversion systems: Trends and applications," *Renew. Sustain. Energy Rev.*, vol. 167, Oct. 2022, Art. no. 112734.
[13] N. Ali, Z. Liu, H. Armghan, and A. Armghan, "Super-twisting sliding mode controller for maximum power transfer efficiency tracking in hybrid energy storage based wireless in-wheel motor," *Sustain. Energy Technol. Assessments*, vol. 52, Aug. 2022, Art. no. 102075.
[14] R. Tiwari, S. Padmanaban, and R. Neelakandan, "Coordinated control strategies for a permanent magnet synchronous generator based wind energy conversion system," *Energies*, vol. 10, no. 10, p. 1493, Sep. 2017.
[15] M. A. Soliman, H. M. Hasanien, H. Z. Azazi, E. E. El-Kholy, and S. A. Mahmoud, "An adaptive fuzzy logic control strategy for performance enhancement of a grid-connected PMSG-based wind turbine," *IEEE Trans. Ind. Informat.*, vol. 15, no. 6, pp. 3163–3173, Jun. 2019.
[16] R. Errouissi, A. Ai-Durra, and M. Debouza, "A novel design of PI current controller for PMSG-based wind turbine considering transient performance specifications and control saturation," *IEEE Trans. Ind. Electron.*, vol. 65, no. 11, pp. 8624–8634, Nov. 2018.
[17] R. Moutchou and A. Abbou, "Control of grid side converter in wind power based PMSG with PLL method," *Int. J. Power Electron. Drive Syst. (IJPEDS)*, vol. 12, no. 4, pp. 2191–2200, 2021.
[18] W. Cao, N. Xing, Y. Wen, X. Chen, and D. Wang, "New adaptive control strategy for a wind turbine permanent magnet synchronous generator (PMSG)," *Inventions*, vol. 6, no. 1, p. 3, Dec. 2020.
[19] M. A. Soliman, H. M. Hasanien, A. Al-Durra, and I. Alsaidan, "A novel adaptive control method for performance enhancement of grid-connected variable-speed wind generators," *IEEE Access*, vol. 8, pp. 82617–82629, 2020.
[20] S. M. Tripathi, A. N. Tiwari, and D. Singh, "Controller design for a variable-speed direct-drive permanent magnet synchronous generator-based grid-interfaced wind energy conversion system using D-partition technique," *IEEE Access*, vol. 5, pp. 27297–27310, 2017.
[21] M. I. Mosaad, H. S. M. Ramadan, M. Aljohani, M. F. El-Naggar, and S. S. M. Ghoneim, "Near-optimal PI controllers of STATCOM for efficient hybrid renewable power system," *IEEE Access*, vol. 9, pp. 34119–34130, 2021.
[22] M. H. Qais, H. M. Hasanien, and S. Alghuwainem, "A novel LMSRE-based adaptive PI control scheme for grid-integrated PMSG-based variable-speed wind turbine," *Int. J. Electr. Power Energy Syst.*, vol. 125, Feb. 2021, Art. no. 106505.
[23] M. A. Soliman, H. M. Hasanien, S. Alghuwainem, and A. Al-Durra, "Symbiotic organisms search algorithm-based optimal control strategy for efficient operation of variable-speed wind generators," *IET Renew. Power Gener.*, vol. 13, no. 14, pp. 2684–2692, Oct. 2019.
[24] N. H. Saad, A. A. El-Sattar, and M. E. Marei, "Improved bacterial foraging optimization for grid connected wind energy conversion system based PMSG with matrix converter," *Ain Shams Eng. J.*, vol. 9, no. 4, pp. 2183–2193, 2018.
[25] M. H. Qais, H. M. Hasanien, and S. Alghuwainem, "Optimal transient search algorithm-based PI controllers for enhancing low voltage ride-through ability of grid-linked PMSG-based wind turbine," *Electronics*, vol. 9, no. 11, p. 1807, Oct. 2020.
[26] A.-A.-A. Mohamed, A. L. Haridy, and A. M. Hemeida, "The whale optimization algorithm based controller for PMSG wind energy generation system," in *Proc. Int. Conf. Innov. Trends Comput. Eng. (ITCE)*, Feb. 2019, pp. 438–443.
[27] M. H. Qais, H. M. Hasanien, and S. Alghuwainem, "A grey wolf optimizer for optimum parameters of multiple PI controllers of a grid-connected PMSG driven by variable speed wind turbine," *IEEE Access*, vol. 6, pp. 44120–44128, 2018.
[28] B. Yang, T. Yu, H. Shu, X. Zhang, K. Qu, and L. Jiang, "Democratic joint operations algorithm for optimal power extraction of PMSG based wind energy conversion system," *Energy Convers. Manage.*, vol. 159, pp. 312–326, Mar. 2018.
[29] M. M. Hato, S. Bouallegue, and M. Ayadi, "Water cycle algorithm-tuned PI control of a doubly fed induction generator for wind energy conversion," in *Proc. 9th Int. Renew. Energy Congr. (IREC)*, Mar. 2018, pp. 1–6.
[30] Y.-S. Kim, I.-Y. Chung, and S.-I. Moon, "Tuning of the PI controller parameters of a PMSG wind turbine to improve control performance under various wind speeds," *Energies*, vol. 8, no. 2, pp. 1406–1425, 2015.
[31] M. H. Qais, H. M. Hasanien, and S. Alghuwainem, "Augmented grey wolf optimizer for grid-connected PMSG-based wind energy conversion systems," *Appl. Soft Comput.*, vol. 69, pp. 504–515, Aug. 2018.
[32] H. M. Hasanien, "Gravitational search algorithm-based optimal control of archimedes wave swing-based wave energy conversion system supplying a DC microgrid under uncertain dynamics," *IET Renew. Power Gener.*, vol. 11, no. 6, pp. 763–770, May 2017.
[33] H. Shutari, N. Saad, N. B. M. Nor, M. F. N. Tajuddin, A. Alqushaibi, and M. A. Magzoub, "Towards enhancing the performance of grid-tied VSWT via adopting sine cosine algorithm-based optimal control scheme," *IEEE Access*, vol. 9, pp. 139074–139088, 2021.
[34] M. F. El-Naggar, M. I. Mosaad, H. M. Hasanien, T. A. AbdulFattah, and A. F. Bendary, "Elephant herding algorithm-based optimal PI controller for LVRT enhancement of wind energy conversion systems," *Ain Shams Eng. J.*, vol. 12, no. 1, pp. 599–608, Mar. 2021.
[35] S. Mirjalili, "SCA: A sine cosine algorithm for solving optimization problems," *Knowl.-Based Syst.*, vol. 96, pp. 120–133, Mar. 2016.
[36] M. H. Qais, H. M. Hasanien, and S. Alghuwainem, "Transient search optimization: A new meta-heuristic optimization algorithm," *Int. J. Speech Technol.*, vol. 50, no. 11, pp. 3926–3941, Nov. 2020.
[37] M. A. Abdullah, T. Al-Hadhrami, C. W. Tan, and A. H. Yatim, "Towards green energy for smart cities: Particle swarm optimization based MPPT approach," *IEEE Access*, vol. 6, pp. 58427–58438, 2018.
[38] G. Zhuo, J. Hostettler, P. Gu, and X. Wang, "Robust sliding mode control of permanent magnet synchronous generator-based wind energy conversion systems," *Sustainability*, vol. 8, no. 12, p. 1265, Dec. 2016.
[39] A.-R. Youssef, A. I. Ali, M. S. Saeed, and E. E. Mohamed, "Advanced multi-sector P&O maximum power point tracking technique for wind energy conversion system," *Int. J. Electr. Power Energy Syst.*, vol. 107, pp. 89–97, May 2019.
[40] M. Qais, H. M. Hasanien, and S. Alghuwainem, "Salp swarm algorithm-based TS-FLCs for MPPT and fault ride-through capability enhancement of wind generators," *ISA Trans.*, vol. 101, pp. 211–224, Jun. 2020.
[41] Z. A. Alrowaili, M. M. Ali, A. Youssef, H. H. H. Mousa, A. S. Ali, G. T. Abdel-Jaber, M. Ezzeldien, and F. Gami, "Robust adaptive HCS MPPT algorithm-based wind generation system using model reference adaptive control," *Sensors*, vol. 21, no. 15, p. 5187, Jul. 2021.
[42] S. D. Ahmed, F. S. M. Al-Ismail, M. Shafiullah, F. A. Al-Sulaiman, and I. M. El-Amin, "Grid integration challenges of wind energy: A review," *IEEE Access*, vol. 8, pp. 10857–10878, 2020.
[43] H. H. H. Mousa, A.-R. Youssef, I. Hamdan, M. Ahamed, and E. E. M. Mohamed, "Performance assessment of robust P&O algorithm using optimal hypothetical position of generator speed," *IEEE Access*, vol. 9, pp. 30469–30485, 2021.
[44] M. Fannakh, M. L. Elhafyani, S. Zouggar, and H. Zahboune, "Performances MPPT enhancement in PMSG wind turbine system using fuzzy logic control," in *Proc. Int. Conf. Electron. Eng. Renew. Energy*. Cham, Switzerland: Springer, 2020, pp. 797–807.

[45] D. Zouheyr, B. Lotfi, and B. Abdelmadjid, "Improved hardware implementation of a TSR based MPPT algorithm for a low cost connected wind turbine emulator under unbalanced wind speeds," *Energy*, vol. 232, Oct. 2021, Art. no. 121039.
[46] H. Shutari, T. Ibrahim, N. B. M. Nor, N. Saad, M. F. N. Tajuddin, and H. Q. A. Abdulrab, "Development of a novel efficient maximum power extraction technique for grid-tied VSWT system," *IEEE Access*, vol. 10, pp. 101922–101935, 2022.
[47] H. Shutari, C.-L. Wooi, H. A. Hamid, M. I. Mousa, W.-S. Tan, and H. Nabipour-Afrouzi, "Modelling and simulation of definite time over current relay for radial systems protection," *J. Adv. Res. Dyn. Control Syst.*, vol. 11, pp. 785–794, Dec. 2019.
[48] H. Q. A. Abdulrab, F. A. Hussin, I. Ismail, M. Assaad, A. Awang, H. Shutari, and P. A. M. Devan, "Hybrid Harris Hawks with sine cosine for optimal node placement and congestion reduction in an industrial wireless mesh network," *IEEE Access*, vol. 11, pp. 2500–2523, 2023.
[49] H. Q. A. Abdulrab, F. A. Hussin, A. A. Aziz, A. Awang, I. Ismail, M. S. M. Saat, and H. Shutari, "Optimal coverage and connectivity in industrial wireless mesh networks based on Harris' Hawk optimization algorithm," *IEEE Access*, vol. 10, pp. 51048–51061, 2022.
[50] H. Abdulrab, F. A. Hussin, A. Awang, I. Ismail, P. A. M. Devan, and H. Shutari, "Optimal node placement and congestion reduction in an industrial wireless mesh network using HHO algorithm," in *Proc. Int. Conf. Future Trends Smart Communities (ICFTSC)*, Dec. 2022, pp. 164–169.
[51] A. Albani and M. Ibrahim, "Wind energy potential and power law indexes assessment for selected near-coastal sites in Malaysia," *Energies*, vol. 10, no. 3, p. 307, Mar. 2017.

HUSSEIN SHUTARI received the B.Sc. degree in electronics and communications engineering from the Faculty of Engineering, Hadhramout University, Yemen, in 2012, and the M.Sc. degree in electrical power system engineering from the School of Electrical System Engineering, University of Malaysia Perlis, Malaysia, in 2018. He is currently pursuing the Ph.D. degree in electrical engineering with Universiti Teknologi PETRONAS, Malaysia. His research interests include renewable energy systems, operation, control, optimization, and MPPT techniques for renewable energy systems.

TAIB IBRAHIM was born in Kedah, Malaysia, in 1972. He received the B.Eng. degree (Hons.) in electrical and electronics engineering from Coventry University, U.K., in 1996, the M.Sc. degree in electrical power engineering from the University of Strathclyde, U.K., in 2000, and the Ph.D. degree in electrical machine design from The University of Sheffield, U.K., in 2009. His employment experience includes Airod (M) Sdn Bhd and Universiti Teknologi PETRONAS (UTP). Currently, he is an Associate Professor with the Department of Electrical and Electronics Engineering, UTP. His research interest includes electrical machines developments to their associated drives.

NURSYARIZAL BIN MOHD NOR received the M.Sc. degree in electrical power engineering from the University of Manchester Institute of Science and Technology (UMIST), U.K., and the Ph.D. degree in electrical engineering from Universiti Teknologi PETRONAS (UTP), Malaysia, in 2009. His areas of specialization are analysis and optimization of large scale power systems and state estimation. He has several publications at his credit. His research interests include power system state estimation, power system analysis, renewable energy, and electrical machine.

HAKIM Q. A. ABDULRAB (Graduate Student Member, IEEE) received the B.Eng. degree (Hons.) in electrical and mechatronics engineering and the M.Sc.Eng. degree (Hons.) in mechatronics and automatic control from Universiti Teknologi Malaysia (UTM), Johor Bahru, Malaysia, in 2013 and 2019, respectively. He is currently pursuing the Ph.D. degree with the Department of Electrical and Electronics Engineering, Universiti Teknologi PETRONAS (UTP), Perak, Malaysia. He was a Teaching Engineer with the Faculty of Engineering and IT, Taiz University, Yemen, from 2013 to 2016. His current research interests include wireless networked control systems, optimization of network deployment, and fault tolerant control.

NORDIN SAAD (Senior Member, IEEE) received the B.S.E.E. degree from Kansas State University, USA, the M.Sc. degree in power electronics engineering from Loughborough University, U.K., and the Ph.D. degree in control and systems engineering from The University of Sheffield, U.K. During his tenure as an Academic Staff with the Faculty of Engineering, Universiti Teknologi PETRONAS, Malaysia, he was awarded several competitive national and international research grants in artificial intelligence, renewable energy and energy systems, electrical drives control, power electronic converters for solar and wind energy conversions, condition monitoring and diagnostic of machines, and networked and industrial wireless communication. His research work mostly encompasses certain issues in electrical drive control and power electronic converters for high-power transmission and low-power applications, which would be important for research in electrical drive systems and sustainable and secure energy. He is currently a Professor with Quest International University, Malaysia, and the Head of the Faculty of Computing and Engineering, School of Engineering, pursuing research in power electronic converters for solar PV and wind turbine systems, modern transportation systems, mechatronics engineering on robotics, flexible automation, and sensor technology. He has filed several patents and written several book chapters and over 150 papers in refereed IEEE, ISI, and Scopus journals and conference proceedings. He has contributed to four books in engineering and sciences. He is a Chartered Engineer (C.Eng.) registered under Engineering Council, U.K., and a member of the Institute of Measurement and Control (MInstMC), U.K.

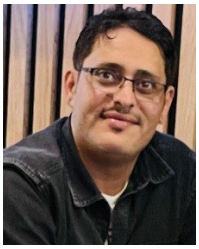

QASEM AL-TASHI received the B.Sc. degree in software engineering from Universiti Teknologi Malaysia (UTM), in 2012, the M.Sc. degree in software engineering from Universiti Kebangsaan Malaysia (UKM), in 2017, and the Ph.D. degree in information technology from Universiti Teknologi PETRONAS, in 2021. He was a Research Scientist with Universiti Teknologi PETRONAS; and a Postdoctoral Fellow with The University of Texas MD Anderson Cancer Center, Houston, TX, USA, where he is currently a Research Investigator with the Department of Physics. His research interests include feature selection, swarm intelligence, biomarker discovery, survival analysis, multi-objective optimization, and artificial intelligence in healthcare. He is a Reviewer of several high-impact factor journals, such as *Artificial Intelligence Review*, IEEE Access, *Knowledge-Based Systems*, *Soft Computing*, *Journal of Ambient Intelligence and Humanized Computing*, *Applied Soft Computing*, *Neurocomputing*, *Applied Artificial Intelligence*, and *PLOS One*. He is an Editor of the *Journal of Applied Artificial Intelligence* (JAAI) and the *Journal of Information Technology and Computing* (JITC).